Turkish Journal of Electrical Engineering & Computer Sciences

http://journals.tubitak.gov.tr/elektrik/

Research Article

Turk J Elec Eng & Comp Sci
(2018) 26: 1541 – 1554

doi:10.3906/elk-1701-136

An integrated approach for the development of an electric vehicle powertrain: design, analysis, and implementation

Özgür ÜSTÜN[1,2], Ramazan Nejat TUNCAY[2,3], Mert Safa MÖKÜKCÜ[1,2], Ömer Cihan KIVANÇ[2,3,*], Gürkan TOSUN[2,3], Can GÖKÇE[1,4], Murat ÇAKAN[1,2]

[1]Department of Electrical Engineering, Faculty of Electrical and Electronics Engineering, İstanbul Technical University, İstanbul, Turkey

[2]Mekatro Mechatronics R&D, İstanbul, Turkey

[3]Department of Electrical and Electronics Engineering, Faculty of Engineering, Okan University, İstanbul, Turkey

[4]Türk Otomobil Fabrikası Anonim Şirketi (TOFAŞ), İstanbul, Turkey

Received: 14.01.2017 • **Accepted/Published Online:** 13.07.2017 • **Final Version:** 30.05.2018

Abstract: Electric motor and power electronic systems are essential elements for the performance and efficiency of electric vehicles (EVs) and hybrid electric vehicles. The inadequacy of the range due to battery limitations is compensated by powertrain solutions and innovative control algorithms. Future targets of electric powertrains are mostly based on weight, space, and efficiency issues. Highly efficient low-volume and light-weight propulsion systems increase the performance of EVs and also enhance their importance as an alternative to internal combustion engine vehicles. In this paper, a detailed propulsion system design study is presented by considering all of the important constraints of the electric powertrain. The design criteria and output, which are opposites of each other, are submitted in terms of their advantages and disadvantages. The tests of all constraints are conducted as a whole and discretely and then the effects of electrical machine and power electronics circuits are presented.

Key words: Brushless DC motor, electric vehicle, hybrid electric vehicle, finite element analysis, computational fluid dynamics, subfractional slot winding, regenerative braking, internal combustion engine

1. Introduction

The impact of electrical vehicles (EVs) is progressively skyrocketing in daily life. This impact is leading the way for research efforts concerning each component in EV powertrains, i.e. the electric motor, battery pack, and power electronic system. However, recent developments about internal combustion engine (ICE) vehicles should not be ignored. Nowadays, CO_2 emission has decreased to around 40% in ICE vehicles. According to reports, CO_2 emission values are down to 250–270 g/km in the USA, 150–170 g/km in Europe, 200–215 g/km in China, and 130–140 g/km in Japan. These values denote that CO_2 emission in new technology vehicles has been reduced [1]. Besides the reduction in emission, an increase in the comfort and performance of ICE vehicles is evident. Engine downsizing, turbocharging, optimized cooling, low friction, start-stop systems, and direct injection are the major developments related to comfort and performance. The most current and popular liquid fuels are fossil fuels; however, even by conservative estimates, the depletion of petroleum reserves will occur in the next 35 years [2]. However, a sudden shift of the vehicle market from ICE vehicles to EVs is not

*Correspondence: cihan.kivanc@okan.edu.tr

realistic while a transition between two technologies is still under way, i.e. hybrid electric vehicles (HEVs). The sales figure of HEVs that are manufactured especially for their increasing range and use in local transportation is encouraging for upcoming EVs [1]. The most important threat for EVs is the range problem that results from the underdevelopment of insufficient battery technology. It is not possible to contest that EVs have the same performance and range criteria as ICE vehicles. However, research and development studies about the powertrain for EVs have focused on the problem of batteries to a certain extent. Encouraging sales numbers of EV and HEV models are somewhat hampered by range anxiety problems due to the limited capacity of the current market batteries. While Tesla Motors is trying to solve the problem by adding more cells to their battery packs, VW and Toyota are looking for answers by considering hybrid powertrains and range extenders [3–5]. The design targets of power electronics and electric machines have changed due to the range extension, mechanical limitations, and constraints of volume and space in automotive applications. Thus, there are different electric propulsion system designs that aim to solve some specific problems. Especially in HEVs, the layout of the merged power system is a serious engineering concern. The propulsion systems of EVs consist of four main components. These are electric motors, power electronic units, the traction drive system, and the battery. The main target of the design of these components is to produce a compact, sophisticated drive train with high thermal endurance. In some future forecast reports for 2020–2030, the volume, weight, and power density are given as the essential factors of EV powertrains. EV technology targets for 2022 in the USA include the reduction of 30% of the vehicle body weight. A propulsion system that was 30 $/kW in 2012 will now be targeted as 8 $/kW in 2022. The main targets are also given as 1.4 kW/kg, 4 kW/L, and 94% efficiency. In the same report, the price reduction of a powertrain with 55 kW to 440 $ is a goal for 2022 [6].

There are various electrical machine structures for the different configurations of EVs. In that sense, induction motors (IM), brushless DC motor (BLDC) motors, switched reluctance motors, and interior permanent magnet synchronous motors (IPMSMs) are used in various EV and HEV powertrain topologies [7–14]. Rare earth permanent magnets (PMs) provide the electrical machines with light weight, increased compactness, and high torque production capacity. However, it should be noted that there is a recent tendency to reduce the usage of rare earth PMs [6]. Power electronic circuits become smaller in size due to the improvement of material and manufacturing technologies. Based on recent advances in the development of FPGA, DSP, and MCU technologies, efficiency-focused algorithms are developed more effectively. The higher speed and higher capacity of computing presented by recent processors, along with their versatile communication abilities, is providing more effective and efficient electric powertrain systems. High efficiency conversion of mechanical energy to electrical energy during braking is the most important advantage for electrical machines compared to ICEs [15]. Up to 20% in energy savings is provided and the driving range is extended with regenerative braking. In addition, the rated shaft speed of the motor can increase 5 to 6 times in the constant power region, i.e. field weakening, by providing machine operation beyond the constant torque region [16]. While this method is applied more effectively by IPMSMs, the extended speed range is about 2 to 3 times the base speed for surface magnet machines [17]. The field weakening capability eliminates the losses due to the adjustable gearbox and clutch system. The main aim of this study is to satisfy near future EV power train targets, i.e. power density, volume, and weight. Along with these targets, a high performance and efficient control system is developed that meets passenger electric car drive requirements. The prototyped EV powertrain performance is tested and investigated and the developed power train is ready to be integrated in the specified car.

2. Fundamental calculation of vehicle traction

The design criteria, power and torque values that are necessary for the design of the propulsion system, are obtained from the vehicle's dynamic model. In Figure 1, the forces that act on the vehicle in the x − direction are shown.

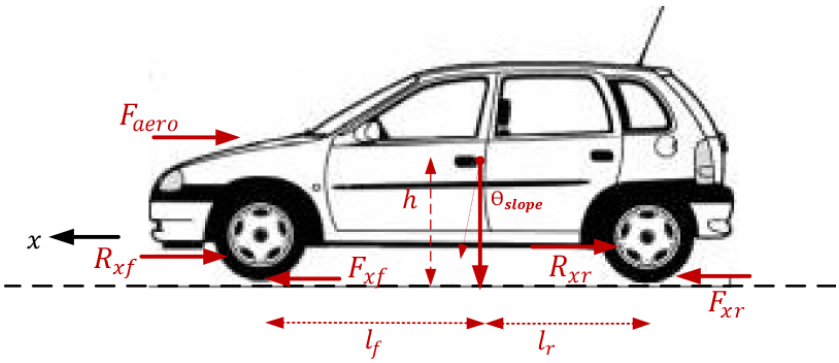

Figure 1. Vehicle forces analysis model.

In Eq. (1), F_{xf} is the wheel longitudinal force of the front wheels, F_{xr} is the wheel longitudinal force of the rear wheels, F_{aero} is the equivalent aerodynamic drag force of linear motion, R_{xf} is rolling resistance of the front wheels, R_{xr} is rolling resistance of the rear wheels, m is weight of vehicle, g is gravitational force, and θ is slope of the road on which the vehicle is driven. A typical city car and the related load effects are shown in Figure 1. The average technical specifications of the selected vehicle are presented in Table 1. The curb weight of the vehicle with an ICE is 880 kg; however, the body weight without the motor and adjustable gearbox is approximately 650 kg, and the predicted weight of the modified EV version with a driver is nearly 1000 kg.

Table 1. Technical specifications of the vehicle.

Power of ICE	44 kW (60 hp)
Empty mass (with ICE)	880 kg
Frontal area	2.08 m^2
Wheel friction coefficient	0.015
Aerodynamic coefficient	0.36
Wheel radius (r)	0.28 m

$$m\ddot{x} = F_{xf} + F_{xr} - F_{aero} - R_{xf} - R_{xr} - mg\sin(\theta) \tag{1}$$

Calculation of the power of the EV is done by considering optimum conditions. Here, V_x is taken as 130 km/h and θ, the slope of the road, is taken as 5°. Rolling resistance due to tire rolling can be calculated by means of the normal load of the vehicle and the counter force distribution on the contact surface of the tire and road. According to approximated calculations, the total force that is needed for the vehicle traction effort is determined as 1320 N at a maximum speed of 180 km/h. Total wheel traction torque for this force is 370 Nm, and the wheel rotational speed is 1700 $\min^{-1}$. For the vehicle to reach a speed of 180 km/h and provide the necessary torque, usage of gear ratio at 4.7:1 is proper because of the required high-speed motor. To reach this speed value, a 70-kW electric motor with 8100 $\min^{-1}$ rated shaft speed is an adequate selection. The required power range to provide highway driving speeds is estimated within a range of 40–60 kW. However, 70-kW motor power is defined to be sufficient by taking into consideration sudden acceleration, uphill climbing and, of course,

target maximum speed. After the calculations, based on resistive forces, 70-kW motor output power and 83-Nm torque output are defined. The prototyped motor is a BLDC motor with rated shaft speed of 8000 $\min^{-1}$. As is known, for EVs, induction motors and IPM synchronous motors are mostly used with superior field weakening capabilities that provide wider operation speed ranges. However, in surface magnet BLDC motors, the field weakening operation is quite problematic. The field weakening operation of a BLDC motor can increase the shaft speed 1.5 or 2 times the rated speed in larger power motors. Because the field weakening operation in BLDC motors is obtained by applying a phase advanced current with current peaks, abrupt current jumps can only be maintained for certain power levels. However, with increasing power values, phase advanced currents will have very high peaks that can be dangerous for the battery system, power electronic system, and motor windings. Therefore, in this study, a BLDC motor is designed and implemented without field weakening, which satisfies all required traction power values over the whole driving speed range. For this purpose, relatively lower current density is selected for the rated current, while higher current densities exceeding 10 A/mm^2 provide enough accelerating and grading traction forces, accordingly. The maximum speed of the EV is defined as 180 km/h by equalizing the traction force to the sum of wind and rolling resistances on flat road cruising at motor-rated power conditions. The motor can fulfil 0–100 km/h acceleration without exceeding the predefined current limit in 7.3 s. However, by applying proper liquid motor cooling, this time can be reduced to 5 s. However, in order to define these overload conditions, the battery pack current providing performance must also be considered. According to the driving conditions, the battery discharge current is taken as 10–12 C. However, maximum discharge current can be demanded for a short period of time. Repetitive current draws for multiple accelerations can limit vehicle performance because of battery overheating. A good but limited solution can be provided by a parallel-connected supercapacitor. By considering these facts, in this study, the motor heating and cooling system design are investigated in detail.

3. Electric motor analysis and design

After the required motor data are calculated, analytical calculations are made for the motor design. As an electric motor, a subfractional slot winding BLDC motor type is selected due to its higher efficiency, easy manufacturing, and lower cogging torque [18–21]. The motor chosen is an inner rotor outer stator BLDC motor with a 12-slot/10-magnet combination [22–24]. An inner rotor BLDC motor is advantageous for indirect drive powertrains compared to an outer rotor BLDC motor because of its low inertia, low mechanical time constants, bearing assembly, and easy integration to the vehicle. A high-quality electric steel with higher relative magnetic permeability is used to form the stator structure. It is expected that the ferromagnetic core provokes high magnetic flux density in low magnetic field intensity, and the iron loss is consequently low. The designed rotor back iron has to be manufactured from high magnetic permeability and low-carbon cold-rolled steel. In order to specify the thickness of the back iron, it is expected that it will create the ampere-turn within reason when the magnetic field moves through this iron. It is important that the core ampere-turn be a small percentage of air gap ampere-turn for enhanced performance. In order to obtain higher torque production, rare-earth PMs with higher energy contribution are used. The SmCo (samarium cobalt) type is chosen because of its high temperature tolerance, especially for higher current demand driving modes, e.g., during acceleration and uphill climbing. According to recent research findings, magnet embracing is applied as 80%, which means that the allocated mechanical arc of the magnet pole is occupied by a combination of 80% permanent magnet and 20% nonmagnetic spacing [25].

To obtain performance superiority, there are different types of winding topologies to increase the efficiency

of BLDC motors and to make the manufacturing process easier. This new type of motor, which uses concentrated windings with different values of slot/pole combinations instead of distributed windings, is called a subfractional slot winding motor. By means of this topology, the BLDC motor provides higher efficiency, performance, and production ease [26]. Due to the utilization of the concentrated windings shown in Figure 2, the inductance value is high and therefore motor short-circuit current is restrained. These types of windings are used in applications that require high torque [27]. In the design, the slot/pole ratio is determined from the formula in Eq. (2), where p is the pole number, m is the phase number, and N_s is the slot number. Another important factor for determining the windings in stator slots is conductor current density. The stator current density should not transcend approximately 5–6 A/mm^2 in the design of the surface-mounted magnet BLDC motors.

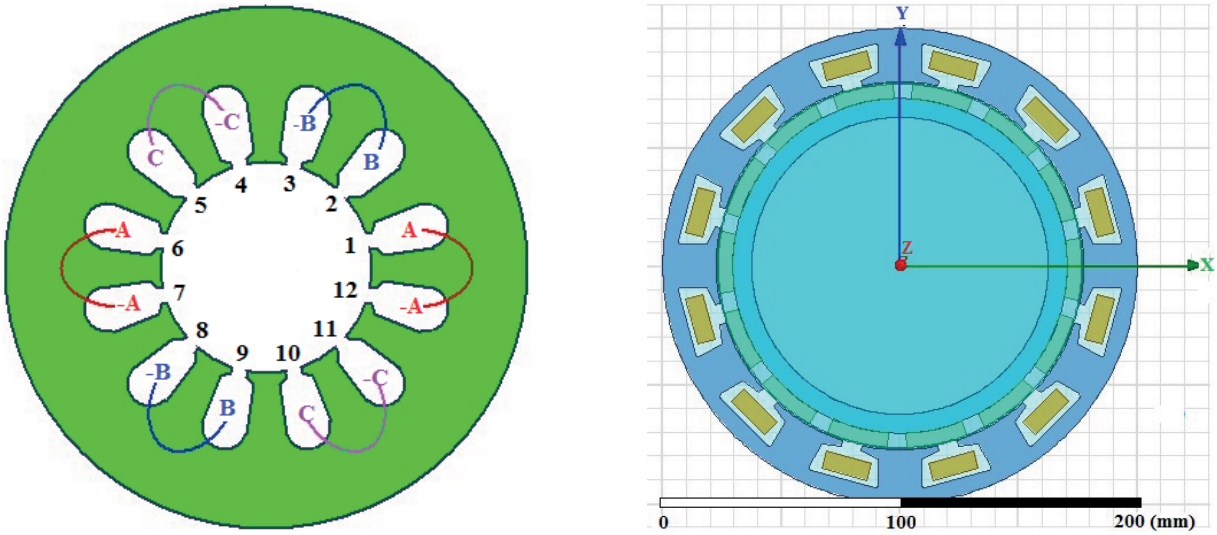

(a) (b)

Figure 2. a) Designed motor schematic, b) motor 2D FEA model.

$$N_{ssp} = \frac{N_s}{2pm} \tag{2}$$

To size the motor, the output power, i.e. the demanded shaft torque and speed, is taken as a design reference point by considering some specific performance values from recent studies. The required torque of the motor is related to rotor diameter D_r, rotor axial length L_r, and constant K, as shown in Figure 3. Torque per rotor volume, which is defined as a measure that is based on rotor dimensions and torque production capacity of motor per unit volume, plays an important role in determining the relationship between motor power and volume. The K constant of the high-performance motor design is between 11.8 and 39 kNm/m^3. In addition, K_{TRV} is between 15 and 50 kNm/m^3 [27].

$$T = KD_r^2 L_r \tag{3}$$

$$K_{TRV} = \frac{4K}{\pi} = \frac{T}{\pi D_r^2 L_r} = \frac{2N_m B_g N i}{\pi D_r} \tag{4}$$

The formulas related to motor sizes are given in Eqs. (3) and (4). The saturation in the yoke and cogs of the slot is considered in the design. The indicative factors that determine the rotor outer and inner diameter are magnets

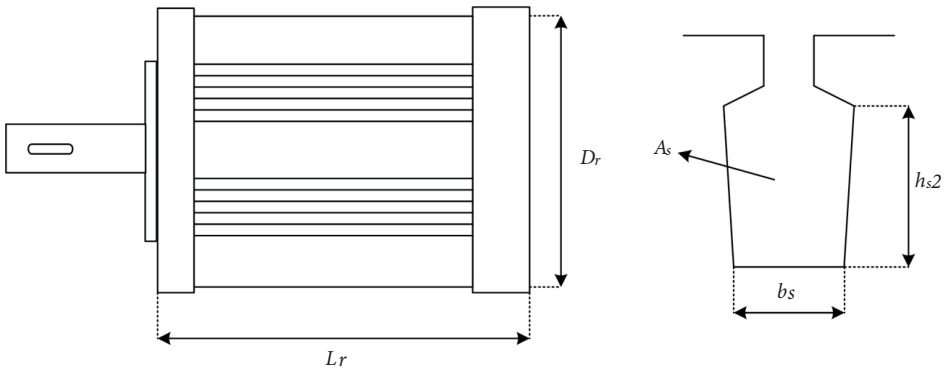

Figure 3. a) Motor main dimensions, b) slot dimensions.

with proper thicknesses that provide the air gap length, magnet back iron thickness, and torque coefficient. The air gap is chosen as the minimum possible size for providing the maximum flux. This quality is defined by the maximum torque per ampere term, which means using the minimum current for maximum torque to diminish copper losses and optimizing motor dimensions. The air gap is characterized by two factors. The first pertains to the quality of magnetic circuit material and structure, which implies maximum torque constant. In other words, when the air gap increases, the magnetic field decreases, i.e. one of the factors of torque production, and so the motor cannot sustain the intended torque. Also, the motor no-load speed increases at the same rate. The second factor that determines the air gap is related to mechanical constraints. In electrical machines that are operated in situations where the motor speed is too high, for a certain value of rotor diameter, the rotational imperfections cannot be decreased below 1 mm. To determine motor performance, wire diameter D_t and the number of turns have important effects. In Eq. (5), A_s is the slot section area, F_s is stator slot filling factor, and N is the number of turns.

$$D_t = \sqrt{\frac{A_s F_s}{N}} \tag{5}$$

Slot types have circular and rectangular structures that depend on slot number and winding type. The slot-filling factor is considered for positioning of the winding to slots during manufacturing. Based on this statement, the slot height, slot tooth width, conductor cross-sectional area, and current density are determined. The stator current density must not exceed 7–8 A/mm^2 as a rule of thumb. The water-cooled motor structure allows the implementation of higher current densities that are common in some EV driving modes. The slot integrity rate is kept below 60% by using the optimum number of turns and the conductor cross-sectional area, which, in turn, prevents the overlapping of windings due to the mechanical constraints of motor thickness. Resistance, R, plays an important role in the determination of copper loss in the motor. Copper loss can be reduced by using the largest possible conductor area. In the meantime, as the wire diameter increases, current density J decreases. The expressions that determine the resistance and current density are shown in Eqs. (6) and (7).

$$R = \frac{\rho L_r N}{\frac{\pi}{4} D_t^2} \tag{6}$$

$$J = \frac{I}{\frac{\pi}{4} D_t^2} \tag{7}$$

In Eq. (6), ρ is the resistivity of conductor material. There is no effect of current density on induced voltage

and inductance, which are changed according to the number of turns of the conductor. The number of turns belongs to one phase N_f, stator area frequency f_s, and fractional pole slotted motor induced voltage, which depends on the $\emptyset$ fundamental air gap flux originating from the magnets. This is given in Eq. (8).

$$E = 2\pi \frac{f_s N_f k_w \emptyset}{\sqrt{2}} \tag{8}$$

The stator inductance value L_s depends on the permeability coefficient of air μ_0, axial length of motor, stator slot depth h_{s2}, and slot width b_s, as shown in Figure 3. The parameter that is the most effective on inductance is the number of turns, and inductance is proportional to the square of the number of turns. The equation defining the stator inductance value is given in Eq. (9).

$$L_s = \frac{\mu_0 h_{s2} L_r (2N)^2}{3b_s} \tag{9}$$

Furthermore, to verify the motor calculations and for design optimization, an analytical simulation is run with ANSYS RMxprt software. The output dataset is given in Table 2. If the output dataset is considered, all calculations are well suited for the needs of the vehicle. The torque value is determined as 86.3 Nm, but with the transmission ratio, it can be considered that the vehicle needs are satisfied. After completing the analytical analysis of the designed electric motor, a detailed electromagnetic FEA is made before the manufacturing process. The numerical analysis that is carried out in ANSYS Maxwell software used a time step of 0.1 ms and a stop time of 30 ms. The 2D electromagnetic FEA model shown in Figure 2 is created and the excitations are given by external circuit application. The output data of the detailed computer-aided electromagnetic FEA are given in the following part of this study. As can be seen from the torque–time variation in Figure 4, by omitting ripples created by the software simulation, the torque value becomes steady at 1.5 ms, and the value of mean torque settles at 95 Nm. Figure 5 shows that magnetic flux density does not exceed 2 T, and this results in lower core losses.

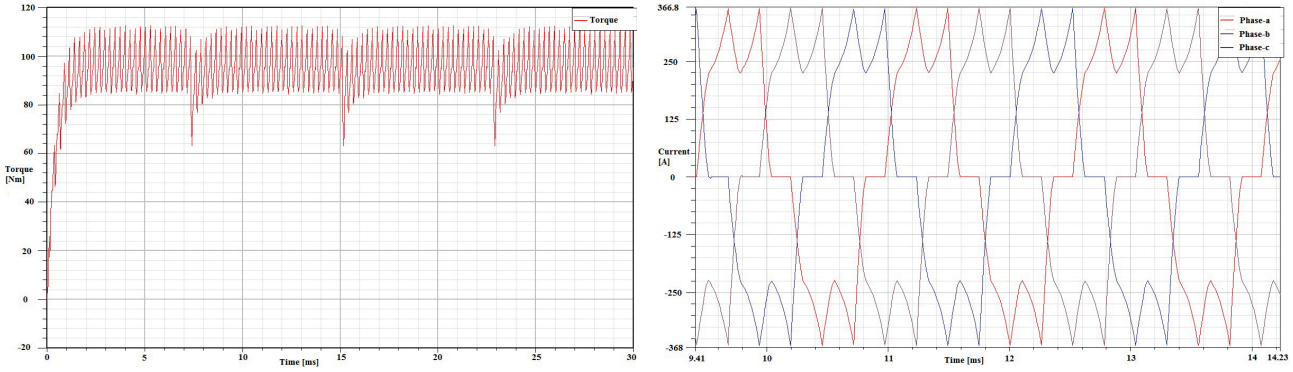

Figure 4. a) Torque–time graph, b) winding current waveforms.

3.1. BLDC motor CFD analysis and configuration of the machine water cooling system

The motor cooling system is one of the most essential components of an EV. Although modern-day electric motor efficiencies are over 90%, depending on their performance conditions, they can dissipate very high heat loads. In such situations, motors should be suitably cooled in order to prevent demagnetization of the magnets and to mitigate winding damage [27]. The numerical analysis carried out in this section of the investigation

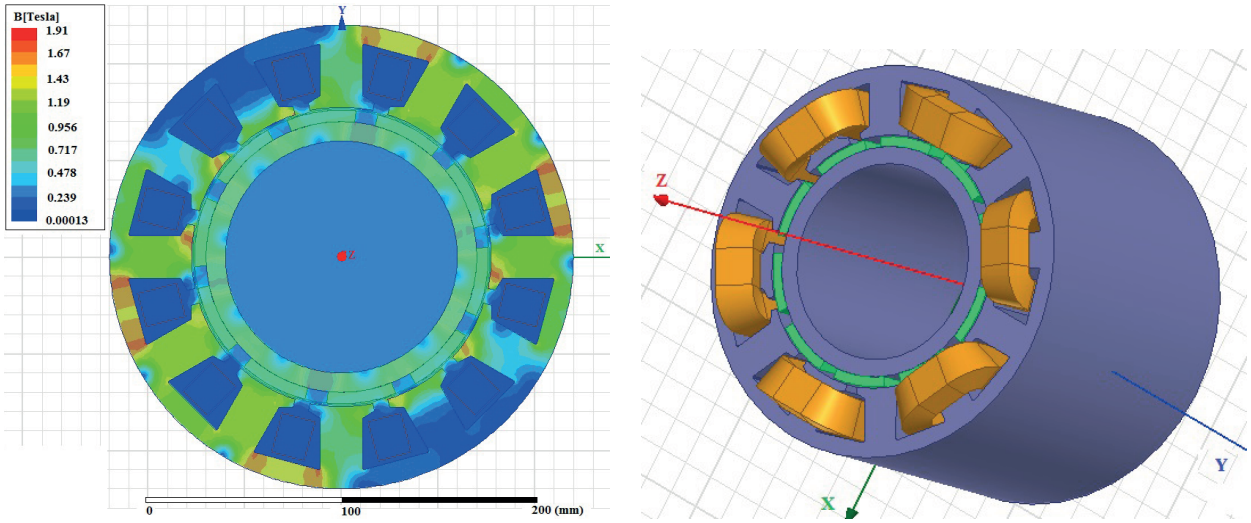

(a) (b)

Figure 5. a) Magnetic flux density graph, b) 3D model of the designed BLDC motor.

Table 2. RMxprt solution data of the electric motor.

Number of poles	10	Rotor yoke flux den. (T)	1.54
Number of stator slots	12	Avg. input current (A)	213.8
Outer diam. of stator (mm)	200	Current density (A/mm^2)	2.27
Air gap (mm)	1.5	Cogging torque (Nm)	5.7
Magnet type	SmCo	Total loss (W)	5917
Voltage (V)	355	Output power (W)	69989.6
Net calc. weight (kg)	42.0421	Rated speed (min^{-1})	7744
Stator teeth flux den. (T)	1.41	Rated torque (Nm)	86.3 (4:1)
Stator yoke flux den. (T)	1.42	Efficiency (%)	92.2

is a result of this necessity. Previous studies and experience in the field impose working conditions that are below 90 °C for a proper functioning of the EV. The research initiative was based on several already proven cooling models. Our specific target, presented in Table 3, was to increase the cooling ability of similar systems via the introduction of geometrically modified new cooling models that are wrapped around the motor casing. The modeled configurations are listed as the serpentine model, manifold model, helical model (long), helical model (short), and helical model with turbulators. Each numerical analysis carried out for the above models was numerically tested with flow rates of 4, 8, 12, and 16 L/s. However, in this paper, only the predictions of the serpentine model CFD will be presented and discussed since lower motor average temperatures were attained with this specific configuration. During the CFD analyses executed using FLUENT software, the ANSYS Workbench was utilized as presented in Figures 6a–6d. This environment helps the user with accurate data connection, as the loss data from electromagnetic analyses were used as input for the CFD analyses shown in Table 4. As can be seen from Figures 6b and 6d, the temperature distribution appears to be quite homogeneous, exhibiting maxima at around 81 °C. Although the analyses carried out for the flow rate of 16 L/min gave lower average casing and stator temperatures, they also caused a much higher pressure drop along the serpentine passages. Therefore, among the four flow rates assessed, 8 L/min was chosen as the best configuration since optimum heat transfer enhancement versus pressure was obtained with this case. The prototyping phases of

the motor are shown in Figures 7a–7d: stator lamination stacking, magnet assembling and gluing, covering the magnets by a plastic jacket, and whole motor assembly, respectively.

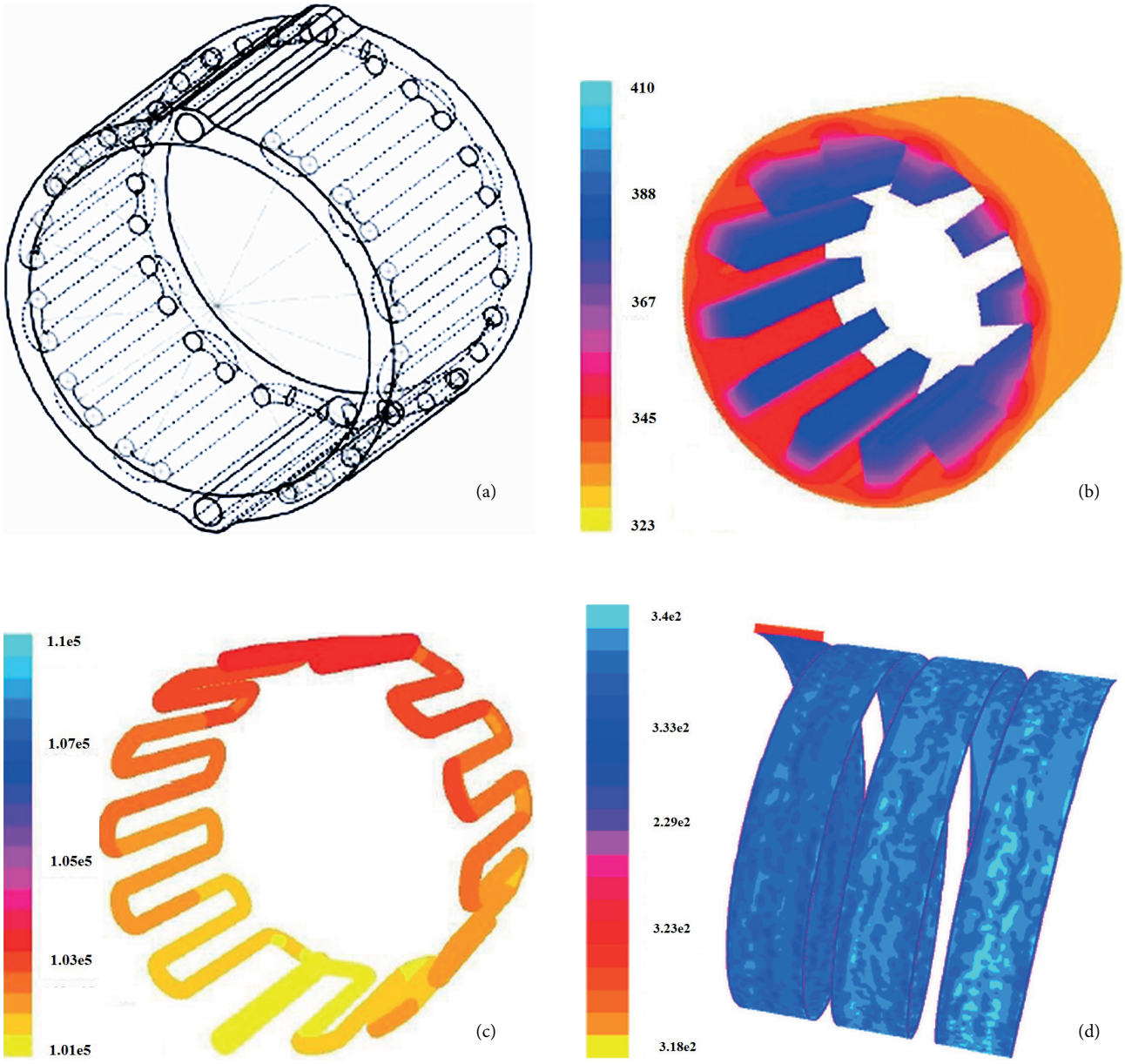

Figure 6. CFD analysis results: a) serpentine-type case, b) serpentine-type case stator temperature [K] distribution (8 L/min), c) serpentine-type case pressure [Pa] distribution (8 L/min), d) motor surface temperature [K] distribution.

Table 3. Motor heat parameters.

Parameter	Value
Frictional loss	809.54 W
Iron core loss	3781.08 W
Armature winding loss	432.44 W

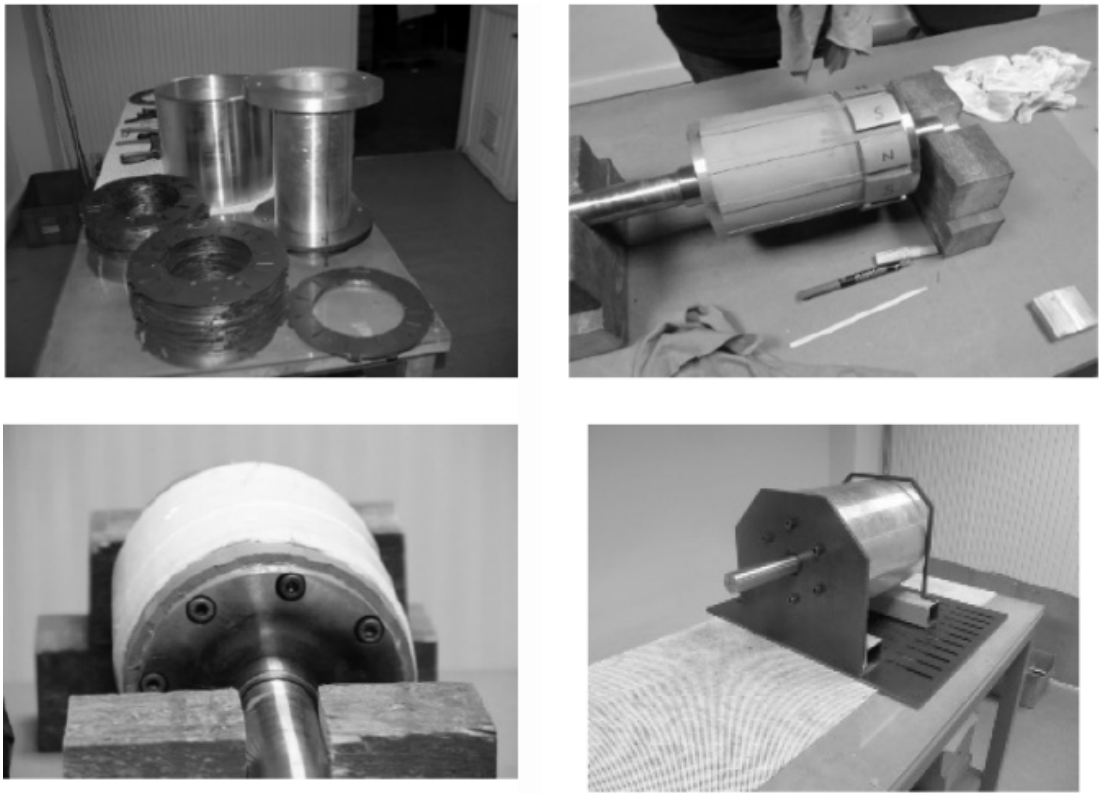

Figure 7. Manufacturing steps of BLDC motor.

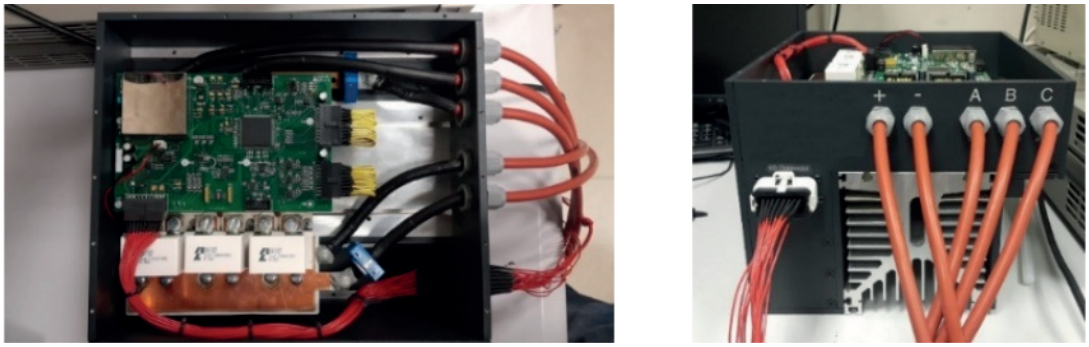

(a) (b)

Figure 8. EPT driver system: a) top view of driver, b) front view of driver.

Figure 9. Experimental test bed (150 kW, 400 Nm).

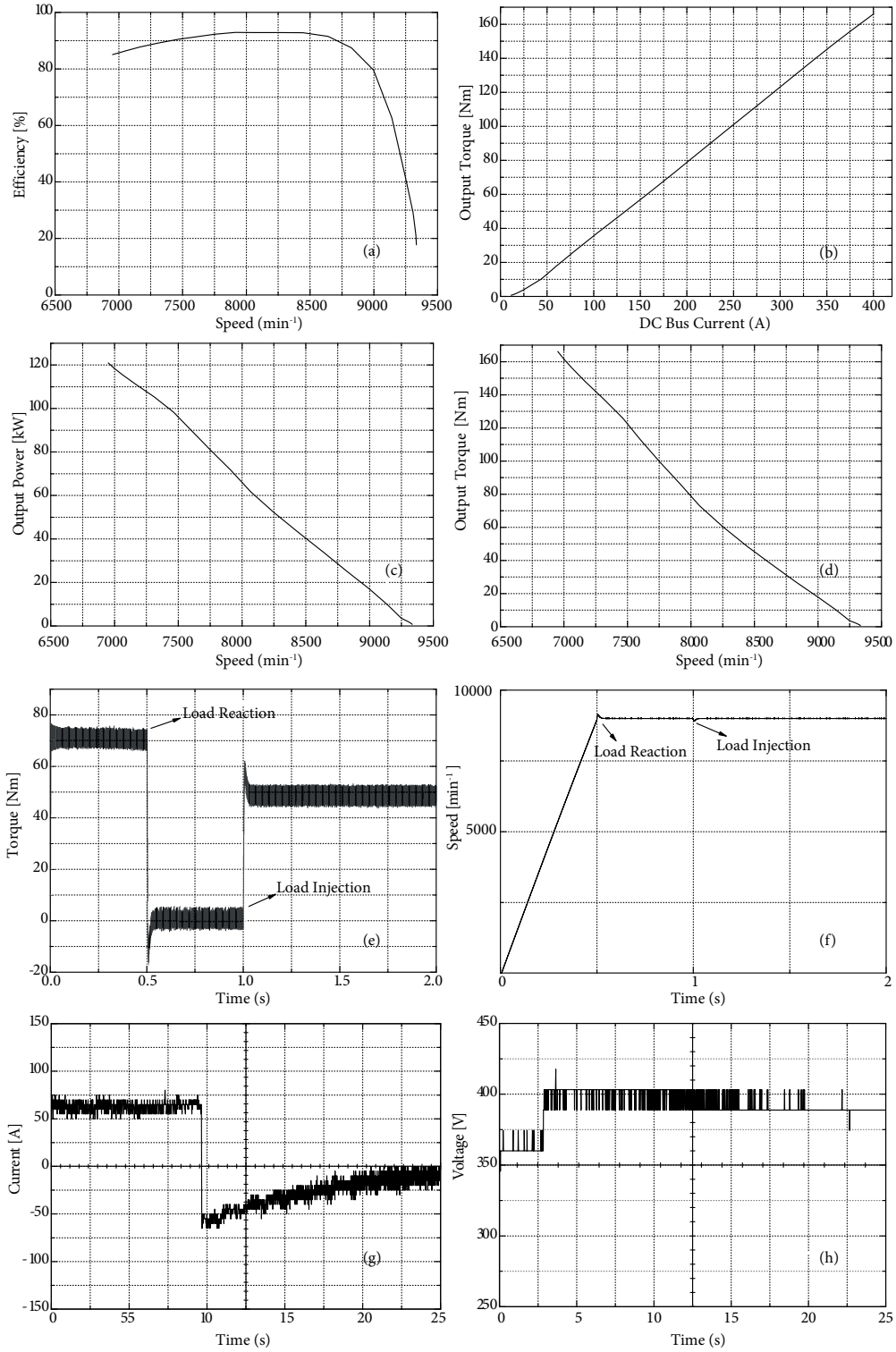

Figure 10. Brushless DC machine test results: a) speed vs. efficiency, b) DC-bus current vs. output torque, c) speed vs. output power, d) speed vs. output torque, e) torque graph of applied load injection and load rejection, f) speed graph of applied load injection and load rejection, g) voltage waveform at the regenerative braking, h) current waveform at the regenerative braking.

Table 4. Boundary conditions and analyses results.

Parameter	Value
Ambient temperature	50 °C
Airside convection coefficient	5 W/m^{2}K
Iron core loss	3781.08 W
Flow rates	4-8-12-16 L/min

4. Power electronic circuit design

The design and manufacturing of the power electronic circuit that is required for BLDC motor driving and the design of the control system were accomplished by special design software. In Figure 8, the top and side views of the designed EPT driver can be seen. For power stage control, a TMS320F28335 digital signal processor was preferred because of its higher processing frequency and compatibility with automotive applications. The electronic circuit boards of the driver were designed by using ALTIUM DESIGNER. In addition, the mechanical design of the driver system was done by considering mechanical constraints arising from under the hood space.

5. Experimental study

BLDC motor and driver prototype performances were analyzed by the dynamometer system shown in Figure 9 (150 kW and 400 Nm) at Okan University's E-Hike Laboratory. The velocity and torque measurements were conducted by a special torque sensor system. The electrical quantities of the motor were monitored by a power analyzer and an oscilloscope. The main performance characteristics and EPT behavior for different operation modes are given in Figure 10.

6. Conclusions and future work

In this study, all propulsion system components of an EV were developed step-by-step from dynamic model calculations to the prototyping phase. Specifically, the effect of the forces on the vehicle and the force distribution were examined. In addition, required traction power, traction force, motor power, and motor torque and shaft speed values were obtained. With the FEA method, a proper BLDC motor was designed in a computer environment and the factors that affect the design were examined. Improvement was obtained by reducing motor size and mass with occasional water cooling. The characteristic curve of the design was examined by a dynamometer loading system. In order to increase the driving range, effective regenerative braking was implemented. For regenerative braking, the motor driver power stage was exploited with no need for any additional circuit. Optimization studies were performed for the vehicle and advanced control software tests are now under way.

Acknowledgment

This work was supported by the İstanbul Technical University (İTÜ) Scientific Research Projects Unit (BAP).

References

[1] Mosquet X, Devineni M, Mezger T, Zablit H, Dinger A, Sticher G, Gerrits M, Russo M. Powering Autos to 2020, The Era of the Electric Car. Boston, MA, USA: Boston Consulting Group Report Press, 2011.

[2] Ehsani M, Gao Y, Gay S, Emadi A. Modern Electric, Hybrid Electric and Fuel Cell Vehicles–Fundamentals, Theory, and Design. Boca Raton, FL, USA: CRC Press, 2004.

[3] Fleming B. Electric vehicle collaboration-Toyota motor corporation and Tesla motors. IEEE Vehicular Technology Magazine 2013; 8: 4-9.

[4] Xiang D, Hu Z, Song Y, Zhang Y. The innovations and implications of the global business models for electric vehicles. In: IEEE Transportation Electrification Asia-Pacific Conference; 31 August–3 September 2014; Beijing, China. New York, NY, USA: IEEE. pp. 1-6.

[5] Yuya M, Takashi K, Nobuyuki M. Design study on hybrid excitation flux switching motor with permanent magnet placed at middle of field coil slot for HEV drives. In: XXII International Conference on Electrical Machines; 4–7 September 2016; Lausanne, Switzerland. New York, NY, USA: IEEE. pp. 2522-2528.

[6] United States Department of Energy. EV Everywhere, Grand Challenge Blueprint. Washington, DC, USA: Department of Energy, 2013.

[7] Rinderknecht S, Meier T. Electric powertrain configurations and their transmission systems. In: Power Electronics Electrical Drives Automation and Motion; 14–16 June 2010; Pisa, Italy. New York, NY, USA: IEEE. pp. 1564-1569.

[8] Krishnamurthy M, Edrington CS, Emadi A, Asadi P, Ehsani M, Fahimi B. Making the case for applications of switched reluctance motor technology in automotive products. IEEE T Pow Electr 2006; 21: 659-675.

[9] Ehsani M, Gao Y, Miller JM. Hybrid electric vehicles: architecture and motor drives. P IEEE 2007; 95: 719-729.

[10] Rajashekara K. Present status and future trends in electric vehicle propulsion technologies. IEEE Journal of Emerging and Selected Topics in Power Electronics 2013; 1: 3-10.

[11] Lu C, Ferrari S, Pellegrino G. Two design procedures for PM synchronous machines for electric power trains. IEEE Transactions on Transportation Electrification 2017; 3: 98-107.

[12] Bostanci E, Moallem M, Parsapour A, Fahimi B. Opportunities and challenges of switched reluctance motor drives for electric propulsion: a comparative study. IEEE Transactions on Transportation Electrification 2017; 3: 58-75.

[13] El-Refaie AM. Motors/generators for traction/propulsion applications. IEEE Vehicular Technology Magazine 2013; 8: 90-99.

[14] Yang Z, Shang F, Brown IP, Krishnamurty M. Comparative study of interior permanent magnet, induction, and switched reluctance motor drives for EV and HEV applications. IEEE Transactions on Transportation Electrification 2015; 1: 245-254.

[15] Gao Y, Chen L, Ehsani M. Investigation of the effectiveness of regenerative braking for EV and HEV. SAE Journal of Passenger Cars 1999; 108: 25-31.

[16] Jahns TM. Flux-weakening regime operation of an interior permanent-magnet synchronous motor drive. IEEE T Ind App 1987; 23: 681-689.

[17] Ehsani M, Rahman K, Toliyat HA. Propulsion system design of electric and hybrid vehicles. IEEE T Ind Electron 1997; 44: 19-27.

[18] Senol S, Ustun O. Design and analysis of a sub-fractional slot concentrated winding BLDCM with unequal tooth widths. International Journal of Applied Electromagnetics and Mechanics 2002; 39: 859-864.

[19] Zhu ZQ, Xia ZP, Wu LJ, Jewell GW. In?uence of slot and pole number combination on radial force and vibration modes in fractional slot pm brushless machines having single- and double-layer windings. In: Energy Conversion Congress and Exposition; 20–24 September 2009; San Jose, USA. New York, NY, USA: IEEE. pp. 3443-3450.

[20] Bianchi N, Pré MD. Use of the star of slots in designing fractional-slot single layer synchronous motors. IEE P-Elec Pow App 2006; 153: 459-466.

[21] El-Refaie AM. High speed operation of permanent magnet machines. PhD, University of Wisconsin, Madison, WI, USA, 2005.

[22] Reddy PB, El-Refaie AM, Huh K, Tangudu JK, Jahns TM. Comparison of interior and surface pm machines equipped with fractional-slot concentrated windings for hybrid traction applications. IEEE T Energy Conver 2011; 27: 2252-2259.

[23] Cros J, Viarouge P. Synthesis of high-performance PM motors with concentrated windings. IEEE T Energy Conver 2002; 17: 248-253.

[24] Salminen P. Fractional slot permanent magnet synchronous motors for low speed applications. PhD, Lappeenranta University of Technology, Lappeenranta, Finland, 2004.

[25] Hanselman DC. Brushless Permanent-Magnet Motor Design, 1st ed. New York, NY, USA: McGraw-Hill, 1994.

[26] Wang J, Atallah K, Zhu ZQ, Home D. Modular three-phase permanent-magnet brushless machines for in-wheel applications. IEEE T Veh Tech 2008; 57: 2714-2720.

[27] Hendershot JR, Miller TJE. Design of Brushless Permanent Magnet Motors, Oxford, UK: Magna Physics Publishing and Oxford University Press, 1984.